JET–P(99)09

G D Conway et al

A Reflectometer for Fluctuation and Correlation Studies on JET

JET–P(99)09

A Reflectometer for Fluctuation and Correlation Studies on JET

G D Conway, G Vayakis[1], J A Fessey, D V Bartlett.

JET Joint Undertaking, Abingdon, Oxfordshire, OX14 3EA UK.,
[1]Present address: ITER-JCT, Naka, Japan.

Preprint of a Paper to be submitted for publication in
Review of Scientific Instruments

May 1999

ABSTRACT

An integrated system of correlation reflectometers have been installed on the JET tokamak. The diagnostic consists of three X-mode, heterodyne, dual-antenna (bistatic), correlation reflectometers. Two of the reflectometers are dual channel systems at fixed frequencies of 75GHz (edge/SOL measurements) and 105GHz (core measurements) with a selectable poloidal (25mm) or toroidal (40mm) antenna separation. The third reflectometer is a two frequency system for radial measurements with one channel fixed at 92GHz and the other swept between 92-96GHz. All three reflectometers operate simultaneously through the same antenna cluster. The diagnostic can provide unique information on the spatial and temporal characteristics of plasma fluctuations. The capabilities of the system are illustrated with a selection of results.

1. INTRODUCTION

Measuring the correlation and propagation properties of turbulent fluctuations is an important step in understanding, and thus optimizing plasma confinement in toroidal magnetic fusion devices. One particular diagnostic technique - correlation reflectometry [1] has proved to be very effective because of its non-perturbing nature and minimal access requirements. Correlation reflectometers fall into two categories. The first are radial correlation systems [2-10] which use two or more microwave frequencies launched from the same antenna, i.e. along the same line of sight or plasma chord. The two microwave beams reflect from plasma cutoff layers at different radial positions; by varying the frequency difference Δf between the beams (e.g. sweeping one of the frequencies) the radial separation Δr can be changed. The radial correlation length L_r is then defined as the separation at which the cross-correlation coefficient between the two reflectometer fluctuation signals falls to 1/e. The second class of correlation reflectometers are transverse systems which measure the toroidal L_t or poloidal L_p correlation lengths [11-14]. Here, two or more microwave beams are launched and received from separate antennas (different plasma chords) spatially displaced either toroidally or poloidally. The two beams have the same frequency, or are very close in frequency, so as to probe the same cutoff layer. Generally the separation of the antennas Δx is fixed so the correlation length has to be extracted from the degree of coherence between the signals with an assumption for the form of turbulence or perturbation [11].

Ideally one would like to measure the correlation and propagation properties simultaneously in the three orthogonal directions - radial, parallel and perpendicular to the magnetic field [9] - or perhaps even form some kind of image of the plasma turbulence and it's evolution, preferably at several radial locations, such as in the edge and core regions of the plasma.

As a step towards this goal a system of three integrated correlation reflectometers have been installed on the JET tokamak. Two of the reflectometers are fixed frequency, dual-channel, X-mode, toroidal/poloidal systems, one operating at 75GHz and one at 105GHz. These two frequencies are chosen to give cutoff layers at sensible positions over the widest range of toroidal

magnetic fields and plasma densities at which the JET tokamak operates. At lower toroidal fields (2.5Tesla) the 75GHz and 105GHz reflectometers have cutoffs in the outboard edge and core plasma regions respectively, while at higher fields (3.4T) the cutoffs straddle the plasma separatrix or the H-mode transport barrier.

The third reflectometer is a dual-frequency radial correlation system with one frequency fixed at 92GHz and the other swept between 92 and 96GHz. This frequency range is a compromise between hardware restrictions and the desire for a reasonable range of spatial separations (a few cm), as well as providing a third radial point between the two toroidal/poloidal systems. All three reflectometers share a common waveguide transmission system and antenna cluster (bistatic geometry), launching horizontally from the low field (outboard) side of the tokamak mid-plane [15].

This paper describes the reflectometer hardware, and specifically a novel heterodyne detection scheme to minimize the number of microwave oscillators in the toroidal/poloidal systems. The waveguide transmission and antenna systems are also described since they critically affect the system design and performance. The behaviour, resolution and performance of the individual reflectometers are discussed in relation to the design criteria and the hardware restrictions. The capabilities of the diagnostics are then illustrated with a selection of results from different operational conditions and plasma fluctuations.

2. FIXED FREQUENCY REFLECTOMETERS

The two toroidal/poloidal reflectometers are similar in design and operation, although not identical in performance. The 75GHz system was built in-house while the microwave hardware section of the 105GHz system was built to a much tighter specification by IRE, Ukraine [16] and hence has a somewhat better phase performance. Figure 1 shows a schematic of the microwave and electrical circuit. The black lines represent waveguide components while electronic components and coaxial cable connections are shown in grey.

There are two separate reflectometer channels, each with a transmitter and receiver waveguide and horn antenna. The transmitted signals are generated by two Varactor tuned Gunn oscillators which are locked together with a constant 10.7MHz frequency difference using a phase locked loop (PLL) circuit. The PLL compares a reference signal derived from mixing samples from both sources, and a crystal oscillator. The frequencies of the two channels are sufficiently close together that they can be considered to be reflected from the same plasma cutoff layer, but far enough apart to allow discrimination by the receivers, even in the presence of broadband (MHz wide) turbulence.

The received signals are down-converted to an intermediate frequency (IF) of 10.7MHz. In a normal heterodyne receiver separate local oscillators (LO) are required for each channel; but the novel feature of this circuit is that the two transmitter oscillators are themselves separated by 10.7MHz and hence can act as local oscillators for the other channel's receiver. Thus

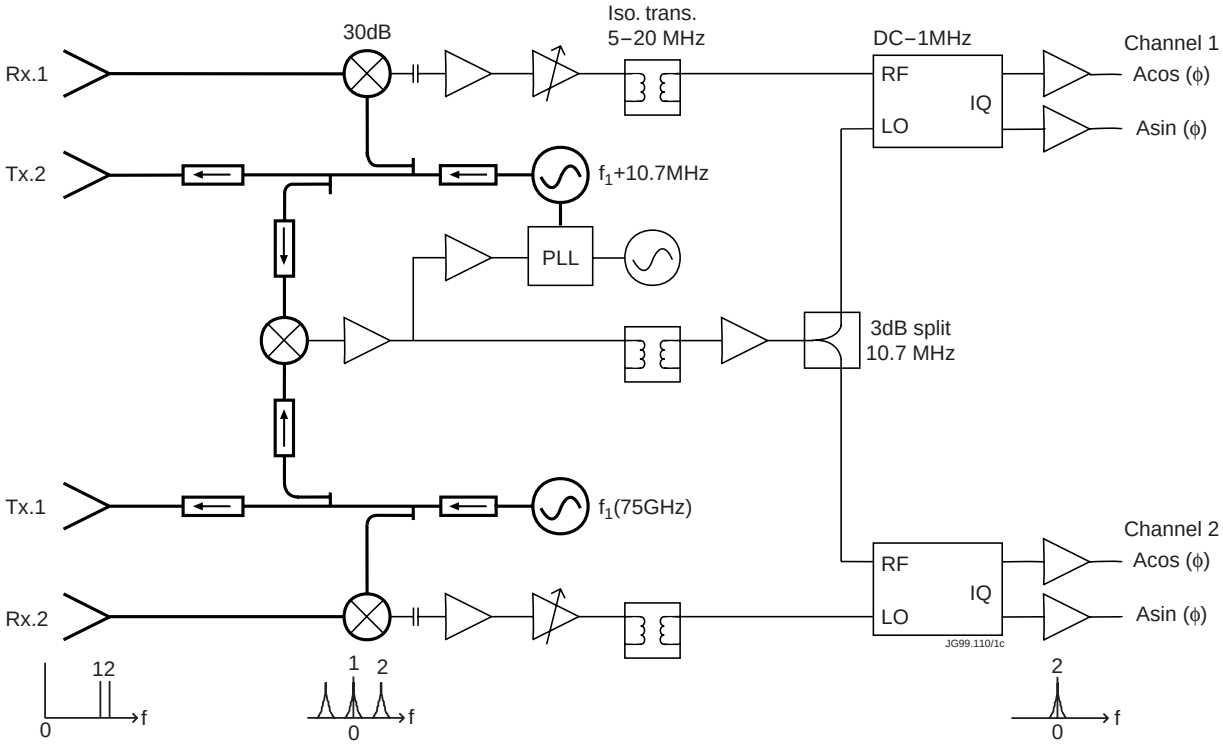

Fig.1: Schematic of the fixed frequency (75GHz or 105GHz) dual channel toroidal/poloidal correlation reflectometer. Thick lines represent waveguide, Thin lines represent electronic circuitry.

only two microwave sources are required instead of the usual four. The receiver operation is illustrated by the spectral schematics along the bottom of Fig. 1. By mixing with the 'Tx.1' source the channel 1 reflected signal is down-converted to zero frequency (homodyne component) while the channel 2 signal is down-converted to the IF of ±10.7MHz (heterodyne components). Likewise in the other receiver mixing with the 'Tx.2' source generates heterodyne components for the channel 1 signal. The homodyne signals are removed by AC coupling to +30dB amplifiers and then via wide-band (5-20MHz) isolating transformers to matched Incident and Quadrature (IQ) detectors (10.7 ± 0.01MHz RF, DC - 1MHz video bandwidth, better than 2% amplitude matching and 2^{o} quadrature accuracy). The IQ's use the derived 10.7MHz reference signal as their LO to generate *I* and *Q* (i.e. *Acosϕ* and *Asinϕ)* signals for each channel.

One advantage of this circuit is that any crosstalk between the channels will appear in the receivers at the homodyne frequency, which is removed. Also, the PLL ensures that frequency drifts in the free running master oscillator (Tx.1) are tracked by the slave oscillator (Tx.2), so only the spectral width of the master oscillator (very small if the oscillator is cavity stabilized) contributes to the phase jitter in the return signals. With a PLL the need for delay lines in the reference signal arms (LO) of the heterodyne mixers is also alleviated.

3. SWEPT FREQUENCY REFLECTOMETER

The radial correlation reflectometer also has two channels, one fixed in frequency at 92GHz and the other swept between 92 and 96GHz. The microwave and electrical circuit is shown

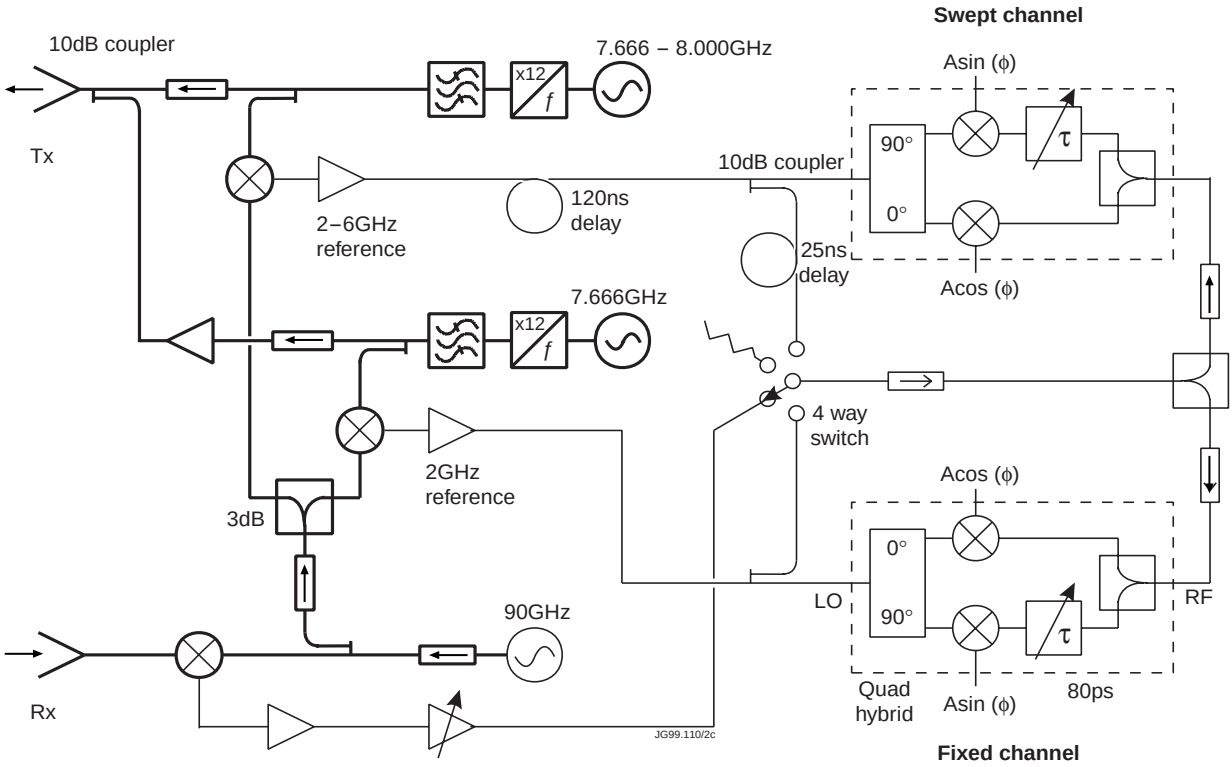

Fig.2: Schematic of the dual frequency 92-96GHz swept radial correlation reflectometer. Thick lines represent waveguide, Thin lines represent electronic circuitry. The dashed boxes enclose the IQ circuit.

schematically in Fig.2, again black represents waveguide components while grey represents electrical. The microwave hardware section was supplied by ELVA-1 Ltd. [17]

The transmitted signals are generated by two separate DRO stabilized transistor oscillators, one fixed at 7.666GHz and the other swept via a digital controller (DAC & PC) over the range 7.666 to 8.000GHz. The signals are up-converted by a factor of 12 in frequency using active multipliers, filtered, amplified (15mW for swept channel, 150mW for the fixed channel) and then combined onto a single launch waveguide using a 10dB directional coupler to equalize the power levels.

The received signal is down-converted to an IF of 2 - 6GHz using a mixer with a 90GHz cavity stabilized Impatt diode LO. The IF signal is amplified and fed via a 4 way switch (used in the calibration procedure described below) to the RF inputs of two IQ demodulator circuits (shown as dashed boxes). One IQ circuit generates a pair of incident and quadrature signals for the fixed channel using a 2GHz reference LO (derived from mixing the 92GHz source with the 90GHz LO), and the other generates IQ signals for the swept channel using a 2 - 6GHz reference derived from the swept source and the 90GHz LO.

It is difficult to make IQ circuits behave ideally across broad IF bandwidths. Here, both the fixed and swept channel IQ circuits are formed from separate (2 - 6GHz) splitters, (1 - 12GHz) quadrature hybrid splitters and mixers. Line stretchers in the 90^{o} hybrid arms allow the phase quadrature of the circuits to be optimized at 2GHz. At other frequencies however there can be substantial variations in the amplitude balance (<10%) and the phase quadrature (10^{o}) -

which also vary with ambient temperature. Fortunately the sources are stable to within 100MHz over a period of hours so the IQ circuits can be calibrated and the *I* and *Q* signals later corrected in software.

This calibration procedure is performed in three steps, as shown for a typical case in Fig.3. Step 1: the four-way switch connects the 'RF inputs' of the IQ circuits to a 50Ω dummy load and the swept source is taken through its full range while recording the DC offsets I_o and Q_o of each channel pair. The top trace of Fig.3 shows that the offsets in the swept channels can vary substantially with the source frequency.

Step 2: the RF inputs are connected to the 2GHz reference (attenuated by 10dB) and a slow, short sweep of the swept source is made around the nominal 92GHz position. When the frequencies of the two sources coincide a resonance is observed in the swept channel IQ outputs. The DAC setting for the swept frequency source at which this occurs is recorded.

Step 3: the RF inputs are connected to the 2 - 6GHz reference signal via a 25ns delay line and the swept source is again taken slowly through its full range. The *I* and *Q* signals from the swept channel IQ circuit show a series of fringes. Integrating the fringes from either signal allows the relative change in the frequency of the source to be measured as a function of the

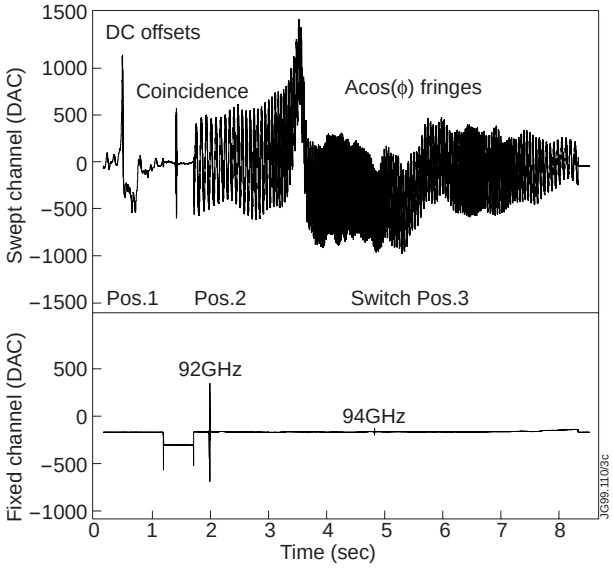

Fig.3: Two Acosϕ time signals, one from the swept frequency IQ (top) and one from the fixed frequency IQ (bottom) of the radial correlation reflectometer during a calibration sweep. The three calibration stages are marked where the RF inputs of the IQ's are respectively connected to (1) a 50Ω dummy load (DC offsets), (2) the 2GHz fixed frequency reference signal (Coincidence) and (3) the 2-6GHz swept frequency reference signal (Acosϕ fringes).

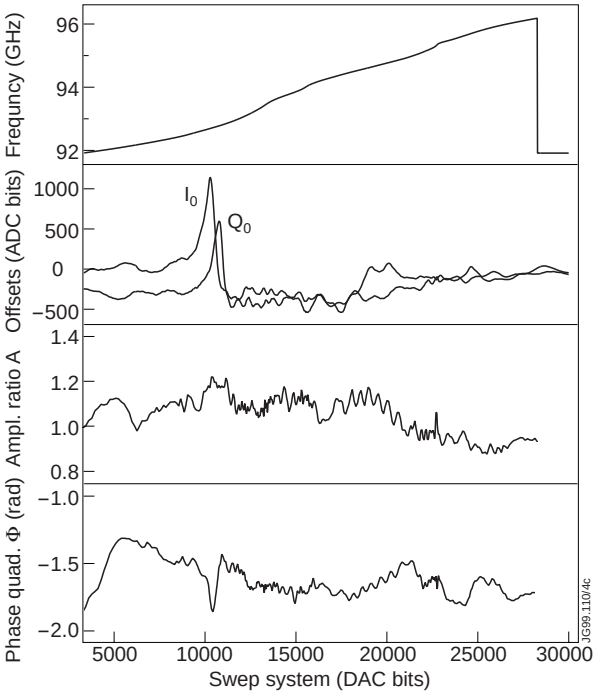

Fig.4: Calibration curves obtained from the calibration sweep shown in Fig.3 for the radial correlation reflectometer swept channel showing (a) swept source frequency, (b) DC offsets I_o and Q_o, (c) amplitude ratio A, and (d) phase quadrature Φ as a function of DAC setting. Note that for the fixed frequency channel I_o, Q_o, A and Φ are single values.

DAC setting. At the same time, the phase difference Φ between the *I* and *Q* signals and the amplitude ratio can be measured (from the Fourier transform of the fringes) and hence a calibration curve obtained.

Figure 4 shows the calibration curves of swept frequency vs DAC setting together with the amplitude ratio, phase quadrature and offsets for the calibration sweep of Fig.3. During the last calibration step observing the fixed frequency IQ outputs allows the positions of crosstalk between the sources at the harmonics of the fixed 2GHz IF frequency to be verified; these are then avoided when the sweep/step pattern is finally programmed into the source DAC.

4. WAVEGUIDE & ANTENNAS

The microwave instrumentation is located outside the JET biological shield wall to prevent radiation damage, so the launch and receive signals must be transmitted to a port in the tokamak mid-plane via four 20m long oversized WG-12A waveguides, as shown schematically in Fig.5(a). Outside the shield wall the separate launch and receive signals are combined onto the WG-12A guides via a system of 3dB and 5dB directional couplers and tapers. Inside the 3m thick shield wall a direct line-of-sight opening for neutron radiation is avoided by using a series of reduced height 'ribbon' waveguide E-plane bends to form a dog-leg.

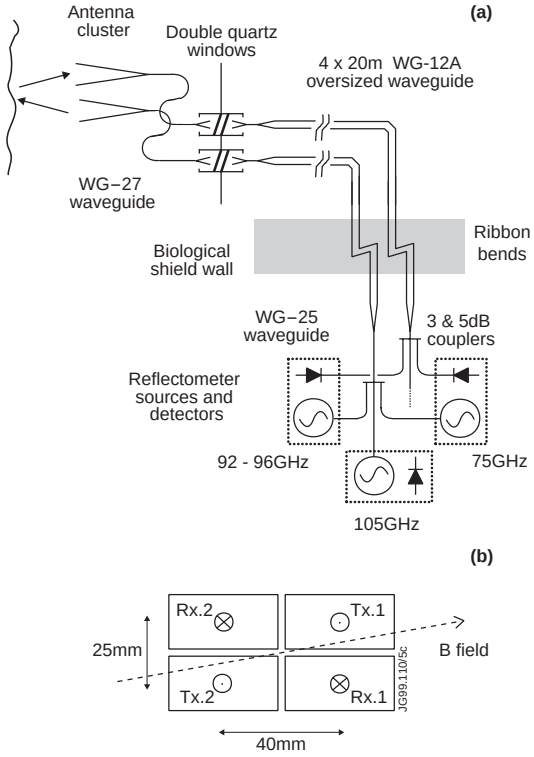

Fig.5: (a) Schematic of the waveguide path (one channel only shown). (b) Layout of the antenna cluster showing positions of transmit and receive horns for a toroidal correlation measurement.

Tappers convert the oversized guides back to fundamental WG-27 just prior to the tokamak vacuum feedthroughs. The feedthoughs consist of pairs of horns (surrounded by anti-crosstalk collars) either side of 15^{o} tilted crystal quartz double windows. Inside the vessel, up to 2m of fundamental waveguide (with several complex twists and bends) connect to four 1m long 25dB gain pyramidal horn antennas with apertures of 40mm by 25mm. The horns are clustered in a rectangular array with centres separated 40mm horizontally (toroidally) and 25mm vertically (poloidally), shown in Fig.5(b), and point radially inward from the tokamak low-field side, slightly above the typical plasma magnetic axis.

The fixed frequency systems use horns on one diagonal of the antenna cluster to transmit the two channels, and horns on the other diagonal to receive. By switching the positions of the two receiving antennas, using special waveguide cross-over sections just prior to the mixers, the

reflectometer channels can be configured to have either a toroidal or a poloidal separation. The swept frequency system launches and receives via one of the transmit and receive antenna pairs.

At the nearest reflection layer (plasma edge: 1 to 1.5m away) the antenna spot size is of the order of 10 to 12cm in diameter (10dB point), which means that the transmit and receive antenna patterns overlap significantly. One of the original aims of the diagnostic was to have as small spot size as possible over the full range of reflection layer locations ($\Delta R \approx 1$m) in order to maximize the sensitivity to transverse perturbation wavelengths [18]. However the antenna design was severely limited by practical constraints. The antenna structure had to fit within the available space of an already crowded JET port, which meant the antenna dimensions had to be rather modest [15]. In addition the antenna cluster was displaced from the vacuum windows, requiring a tortuous path of fundamental waveguide within the vessel. Taken with the requirement for a wide microwave frequency coverage these considerations lead to the selection of an X-mode launch.

5. DATA ACQUISITION & SIGNAL CONDITIONING

In the current implementation the diagnostic employs three separate data acquisition systems, each with a different purpose. The first is a fast sample rate system (up to 2MHz) consisting of three parallel transputers controlled by a PC. The PC also controls the programmable frequency DAC for the radial correlation reflectometer. Currently up to 4Mbyte of data can be collected from up to 15 separately triggered time windows. This allows multiple 'snap-shots' of the behaviour of the high frequency turbulence during a single plasma discharge. The second acquisition system, called CATS [19], simultaneously digitises signals from a variety of diagnostics (soft X-ray cameras, ECE, magnetics, D_α etc.) using a common clock for up to 2 seconds at 1MHz. This system is useful for studying global events such as ELMs and coherent MHD modes. The third acquisition system is a slow (few kHz) 32kbyte CAMAC based digitiser which provides an indication of the level of reflected power (carrier strength) and the overall fluctuation level during an entire plasma discharge. Here pairs of $A\sin\phi$ and $A\cos\phi$ signals from each channel are squared, added, averaged and then square-rooted using analogue CRMS (complex root mean squarer) circuits. The RMS signal is then split, one part low-pass filtered (DC to 10kHz) to give the carrier strength, and the other part high-pass filtered (10 to 100kHz) to give the fluctuation level.

The raw I and Q signals need to be corrected to remove the DC offsets, phase deviations and amplitude imbalances etc. This is performed after digitization using

$$A\sin\phi = Q - Q_o \tag{1}$$

$$A\cos\phi = \frac{I - I_o}{\mathsf{A}\sin\Phi} - \frac{Q - Q_o}{\tan\Phi} \tag{2}$$

where A is the amplitude ratio, Φ the phase quadrature, I_o and Q_o the DC offsets obtained from the calibration for each channel and frequency. The phase and amplitude fluctuations can then

be separated using the quadrature nature of the signals, or the signals can be combined to form a complex amplitude $A\exp(i\phi)$ signal, depending on the analysis to be performed.

6. SYSTEM PERFORMANCES

The performance of each system depends primarily on the frequency stability of the microwave sources. For the 75GHz system the 3dB spectral line-width of the Gunn oscillators is <100kHz, while for the 105GHz system it is <10kHz. A 10kHz line-width translates to a negligible phase jitter ($<0.2^{o}$) over the 40m round trip to the plasma and back.

The swept frequency source in the 92 - 96GHz system however has a broader line-width of <500kHz. Therefore a 120ns delay line is required in the 2 - 6GHz reference line to reduce the several degrees of phase jitter that would otherwise result from the plasma arm delay. This delay line however introduces a small phase jitter due to the 5kHz line-width of the 90GHz oscillator, but this is comparable to the phase jitter of the fixed 92GHz source (line-width of <20kHz) which has no delay line. In this way the phase noise (FM) at the output of both the swept and fixed channels is equalized at a level of a fraction of a degree over the 1MHz video bandwidth.

The swept frequency system can be swept rapidly (400MHz/μsec) but it was principally designed to operate in a frequency stepped mode so as to avoid waveguide resonances. The limiting factor in the step rate is the 10μs settling time of the DAC and the driver electronics. With careful calibration the system can operate reliably with a frequency separation Δf of less than 20MHz.

The oversized waveguides have a single pass attenuation of typically around 9dB, while for the fundamental guide sections it is approximately 6dB. The total round trip attenuation however is closer to 60dB when the plasma reflection and scattering is included. This demands good isolation (i.e. minimal cross-talk) between the transmitter and receiver. In practice the 75GHz system achieves greater than 90dB isolation, and the 105GHz and 92 - 96GHz systems greater than 110dB. The waveguides tend to be more lossy at the lower end of the microwave band requiring more launch power for the 75GHz system, ≈40mW, compared to 23mW for the 105GHz system. The signal to noise ratio (s/n) for all the systems is typically greater than 36dB, which is more than sufficient for reliable measurements. An example IF spectrum from one channel of the 75GHz reflectometer recorded during the ohmic phase of a plasma discharge is shown in Fig.6.

The gains of the IF amplifier chains are adjusted so as to use the maximum dynamic range of the ADCs, however, the signal levels can also vary by 30dB or more due to variations in the degree of reflection. Typically the plasma axis is located some 20cm below the antenna cluster leading to substantial scattering and refraction of the reflected beams due to vertical tilting of the cut-off layers. The degree of cut-off layer tilt depends on the radial position of the layer, the plasma axis height and the plasma shaping, e.g. triangularity, all of which vary dynamically during a discharge. For example Fig.7 shows (a) the mean reflected microwave power (carrier

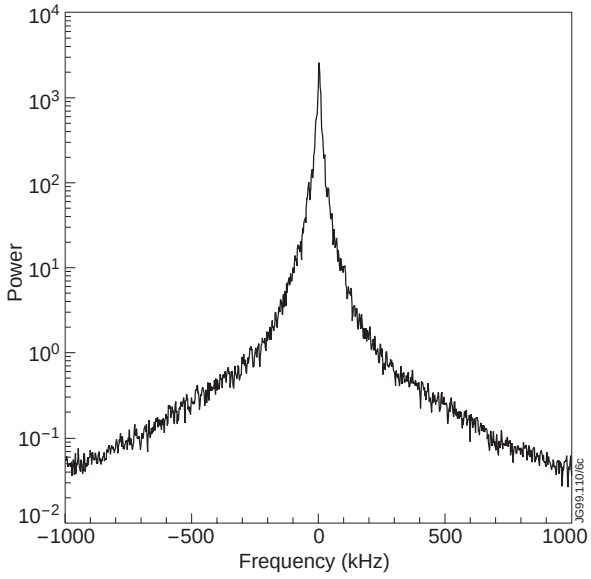

Fig.6: Typical IF spectra from a 75GHz channel showing a dynamic range in excess of 40dB during the ohmic phase of a plasma discharge.

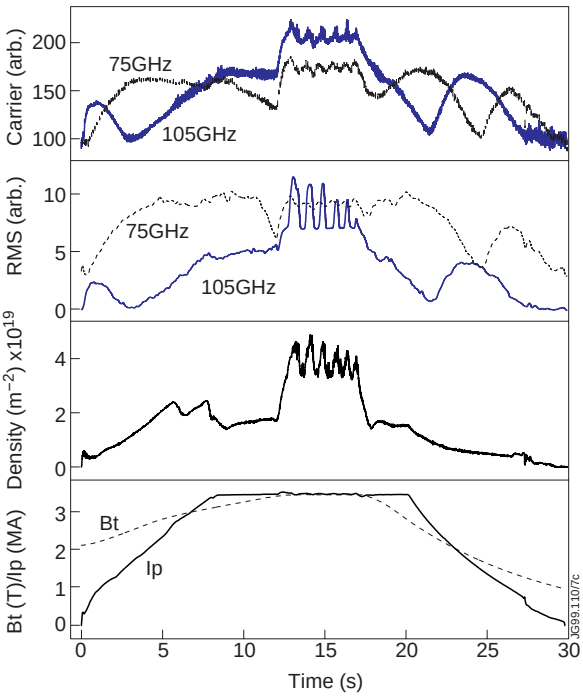

Fig.7: Evolution of (a) mean reflected microwave power (carrier strength), (b) RMS fluctuation levels (from 10 to 100kHz) from a 75GHz (light) and 105GHz (dark) reflectometer channel; together with (c) line integrated central plasma density, and (d) the plasma current Ip and toroidal field Bt during a typical H-mode discharge (shot #43920). Note 'blips' in the NBI power cause corresponding variations in the reflectometer signals.

strength) and (b) the RMS fluctuation level from 75GHz and 105GHz channels through the ohmic, X-point and neutral beam heated phases of a H-mode discharge. The carrier strength improves as the cut-off layers move out during the beam heating phase, shown by (c) the core line averaged density, and falls during beam drop-outs. Observations also confirm that the lower the axis and the higher the triangularity the poorer the reflection.

The magnetic field pitch angle θ relative to the horizontal can be up to 18^{o} at the plasma edge, which, as well as having implications for mode conversion, also affects the measured correlation properties. When $\theta \neq 0$ the toroidal L_t and poloidal L_p correlation lengths contain components of both the parallel $L_{\|}$ and perpendicular $L_{\perp}$ lengths. However previous observations [11] indicate that $L_{\|}$ is of the order of metres while $L_{\perp}$ is expected to range from a few mm to several cm. In this case, $L_t = L_{\perp}/\sin\theta$ and $L_p = L_{\perp}/\cos\theta$. When the reflectometers are configured with a poloidal separation the signal correlation is usually very poor (10 to 20%) which is most likely due to L_p being comparable to, or smaller than the 25mm antenna separation. As expected, the toroidal configuration gives much higher correlation levels of 40 to 80%. This highlights the compromise between the desire for optimal antenna separations, i.e. not too large, and large antenna dimensions to obtain small spot sizes and hence short wavelength sensitivity.

7. ILLUSTRATIVE RESULTS

A wide range of coherent MHD modes and turbulent fluctuation phenomena have already been investigated using the reflectometer system [20,21]. However four examples are selected to illustrate the unique features afforded by multiple radial and toroidal channels.

7.1 Radial correlation of turbulence bursts

The first example demonstrates the value of separating the phase and amplitude fluctuations when measuring correlation lengths. Fig.8 shows contour plots of the γ^2 coherence spectra as a function of time (moving FFT) between (a) the phase and (b) the amplitude fluctuation signals from two fixed radially separated channels (92.0 and 92.5GHz). The spectra show bursts of enhanced broadband coherence (f < 400kHz). In each burst the coherence is stronger between the amplitude fluctuations. Such intermittent variation is common in JET discharges and often has a period as short as a few ms. In this case rather than attempting to measure the whole radial correlation profile using fast frequency sweeping a two point correlation technique is used. Measurement theory [22] gives expressions for the mean and mean square of the *k* spectrum

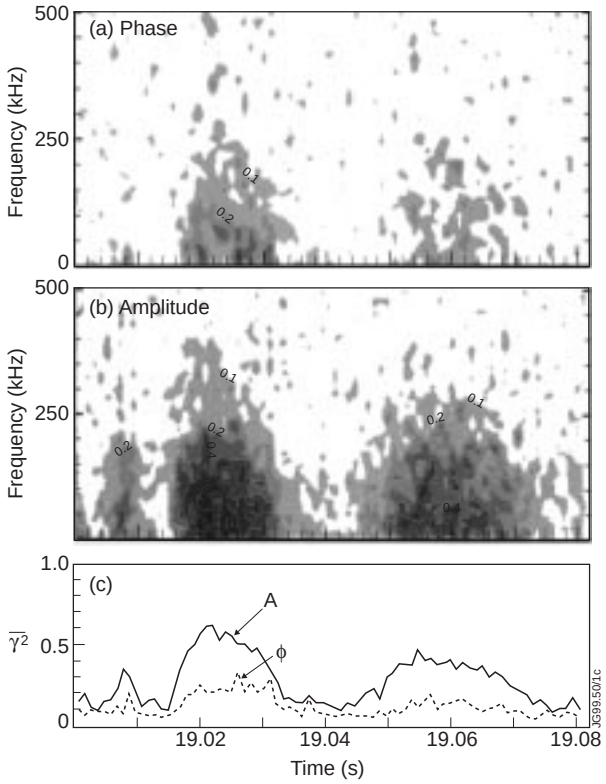

Fig.8: Contour plots of coherence $\gamma^2(\omega)$ spectra vs time for (a) phase fluctuations and (b) amplitude fluctuations between two radially separated channels (92.0 and 92.5GHz → Δr ≈ 2.5mm), during the H-mode phase of shot #39625, and (c) the frequency averaged 'coherency' squared γ2 vs time for phase (dashed line) and amplitude (solid line) fluctuations. The mean cutoff layer is in the plasma edge at r/a ≈ 0.9

$$\bar{k}(\omega) = \Theta(\omega)/\Delta x \tag{3}$$

$$\overline{k^2}(\omega) = 2\{1-\gamma(\omega)\} / \Delta x^2 \tag{4}$$

(provided $k.\Delta x < \pi/2$) where $\Theta(\omega)$ is the cross-phase and $\gamma(\omega)$ the coherence spectra [23]. The *k* spectrum width σ_k is then

$$\sigma_k = \sqrt{\overline{k^2} - \bar{k}^2} \tag{5}$$

For Gaussian turbulence the spectral width is related to the correlation length $L_r = \sqrt{2/\sigma_k}$. With a cutoff layer separation $\Delta x \rightarrow \Delta r = 2.5$mm obtained from a flux surface reconstruction (EFIT), density profiles from a Lidar Thomson scattering diagnostic, and the frequency averaged 'coherency' (Fig.8(c))

$$\bar{\gamma} = \frac{\sum \gamma(\omega) S(\omega)}{\sum S(\omega)} \tag{6}$$

where $S(\omega)$ is the spectral intensity, radial correlation lengths of L_{rA} = 5.0mm and $L_{r\phi}$ = 3.5mm are obtained for the amplitude and phase signals. The discrepancy between L_{rA} and $L_{r\phi}$ is not unexpected. A 2D simulation model [24] suggests correction factors of

$$L_r \approx L_{r\varphi}\left(\frac{\phi_{rms}}{\pi/3}\right)^{\sqrt{3}} \text{ and } L_r \approx \sqrt{2} L_{rA} \tag{7}$$

With ϕ_{rms} = 90^o, these corrections give a consistent radial correlation length of 10mm during the burst and L_r < 2mm in between. The main errors in L_r arise, predictably, from uncertainties in Δr.

7.2 Toroidal propagation velocities

As well as correlation lengths, two point measurements can give propagation velocities and directions. Figure 9 shows the $k(\omega)$ dispersion curves (equation 3) from edge turbulence during (a) ohmic and (b) 6MW ICRF heated ELM-free H-mode phases of shot #38474. The dashed line is the dispersion curve from phase fluctuations and the solid line from amplitude fluctuations with a toroidal separation of Δx = 40mm. The linear dispersion region shows an increase in the toroidal propagation velocity $v = \omega/k$ (in the laboratory frame) from around 18kms^{-1} in the ohmic phase to over 40kms^{-1} in the H-mode. The level of edge and core fluctuations also rise (a side effect of the intense RF heating in this shot) and the toroidal correlation length decreases from over 60mm to less than 40mm.

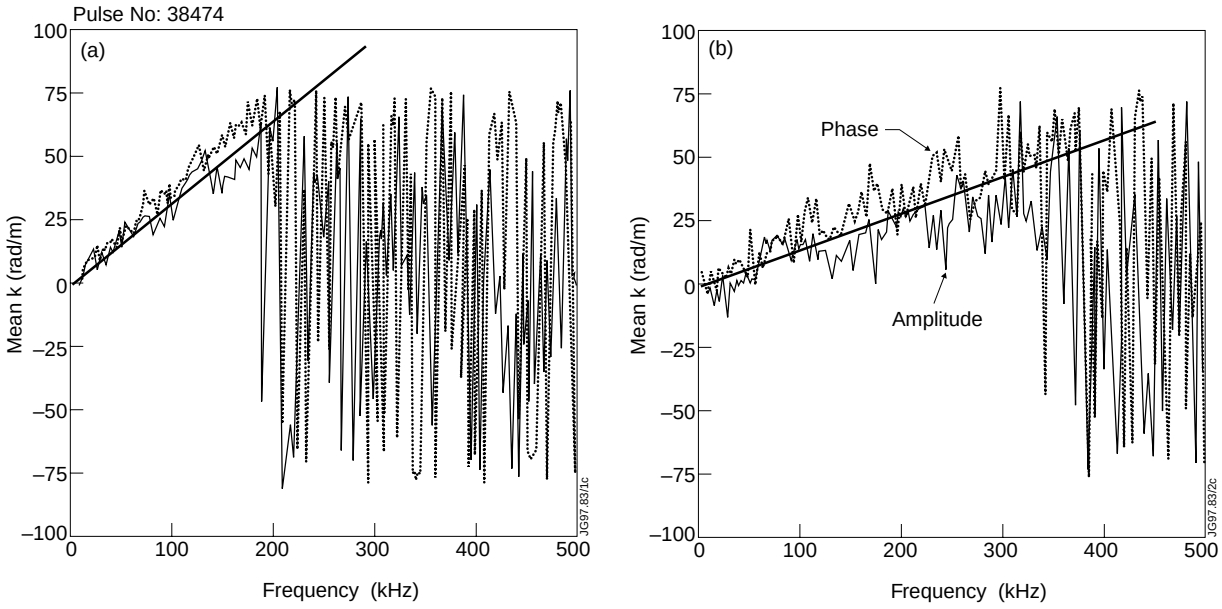

Fig.9: Wavenumber - frequency spectra (dispersion curves) of edge turbulence during (a) the ohmic and (b) 6MW ICRF heated H-mode phases of shot #38474.

During NBI heating the edge propagation velocity often exceeds 150kms^{-1} and generally match plasma rotation velocities measured with a charge exchange diagnostic [6]. Simultaneous measurements with the 75 and 105GHz systems also indicate radial shearing in the toroidal velocity in many discharges. In shot #38474 the phase and amplitude signals give roughly similar velocities, but this is not always the case. Many examples have been recorded where the phase signals give a slower propagation velocity than the amplitude signals. This may be an artifact of the diagnostic technique, which requires further investigation.

7.3 Coherent modes

The next example is of a coherent mode. Figure 10 shows spectra recorded at three radial positions, (a) $r/a \approx 1$ (75GHz), (b) $r/a \approx 0.9$ (92GHz) and (c) $r/a \approx 0.8$ (105GHz) just as the ICRF and neutral beam power are ramping down in the ELMy H-mode discharge #38882. Outside the separatrix, (a) there is only large amplitude low frequency turbulence, but inside the separatrix (b) there is a strong 120kHz mode which extends inward radially for more than 100mm (c). There is also a 220kHz mode but this is more localized to the edge. Strong MHD modes often appear at the termination of an H-mode.

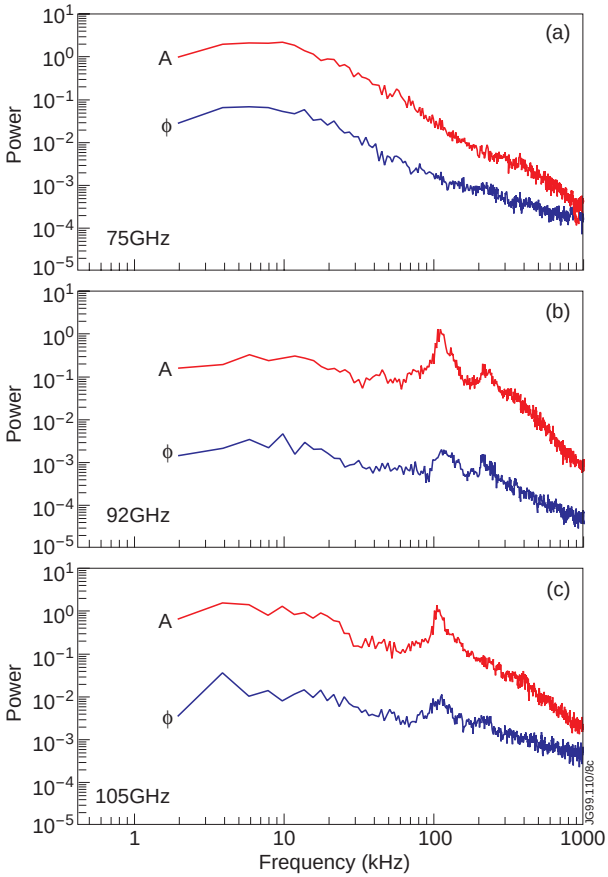

Fig.10: Three spectra showing a strong MHD mode at 120kHz in the phase and amplitude fluctuations from (a) r/a ≈ 1.0 (75GHz), (b) r/a = 0.9 (92GHz) and (c) r/a = 0.8 (105GHz) for JET shot #38882, just as the NBI and ICRF heating switch off.

The 120kHz mode is extremely coherent, as shown by the γ^2 coherence spectra in Fig.11 between (a) between two channels at $r/a = 0.8$ with a toroidal separation of 40mm, and (b) the channels at $r/a = 0.9$ and 0.8 with a radial separation of about 100mm. Between the radially separated channels the cross-phase is zero, which indicates no radial propagation. The toroidal cross-phase however shows a linear dispersion relation with a phase velocity of around 180kms^{-1} which gives a k of about 5radm^{-1} at the f_{mode} =120kHz peak. This phase velocity matches the plasma toroidal velocity $v = \omega_{rot}R$ = 185kms^{-1}, where ω_{rot} = 50krads^{-1} is the toroidal rotation frequency measured with the charge exchange spectrometer at a radius of 3.7m ($r/a \approx 0.8$). Assuming the MHD mode is rotating with the plasma a toroidal mode number

n of 15 is obtained from $f_{mode} = \omega_{rot} /2\pi \times n$. This n number also matches the results obtained from toroidally spaced magnetic pickup coils. The magnetics also indicates that the mode peak coincides with a q = 2 rational surface. Once the n number is known the wavelength is then given by $\Lambda = 2\pi R/n = 1.55$m, or $k = 4.1$radm^{-1}, which again agrees well with the reflectometer.

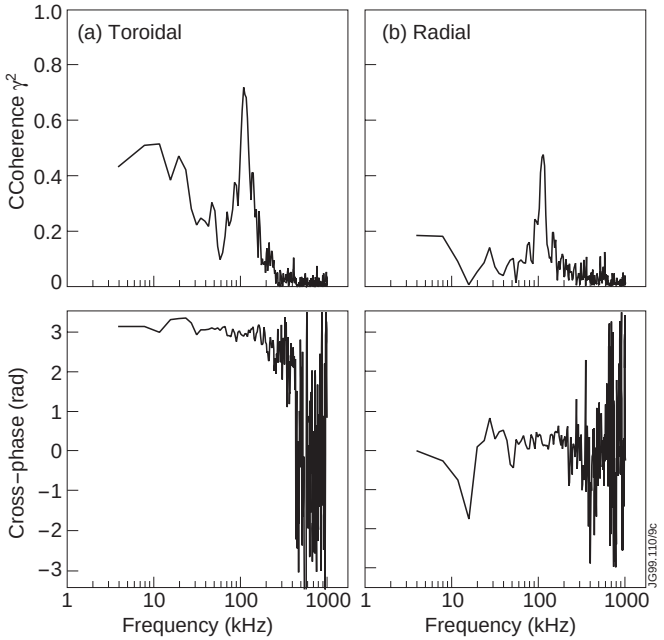

Fig.11: The γ^2 coherence and cross-phase spectra for the coherent MHD mode of fig.10 (shot #38882), between (a) the two 40mm toroidally separated channels of the 105GHz reflectometer, and (b) between channels of 92 and 105GHz reflectometers with a radial separation of about 100mm.

7.4 Edge localized modes

Edge Localized Modes (ELMs) are a common feature in H-mode plasmas. Figure 12 shows a contour plot of the time-delayed cross correlation coefficient between amplitude fluctuations from two channels of the 75GHz reflectometer (toroidal separation Δx = 40mm) during the ELMy H-mode phase of shot #38102 where the cutoff layer is just inside the separatrix. The D_α signal above the contour plot shows two type-I ELMs. Between the ELM events there is a narrow ridge of high correlation which corresponds to broad band turbulence, as shown in the accompanying power spectra. The peak in the correlation is displaced from zero time delay giving a toroidal propagation velocity of 20kms^{-1}.

During the ELM event, indicated by the D_α burst, the toroidal coherence is completely disrupted, and the turbulence level drops, as shown by the second power spectrum. Also during the ELM, and after, the raw reflectometer phase signal displays many fringes indicating a very rapid (on the scale of microseconds) and a very large (several cm) radial movement of the cutoff layer. The phase nearly always increases suggesting an inward movement.

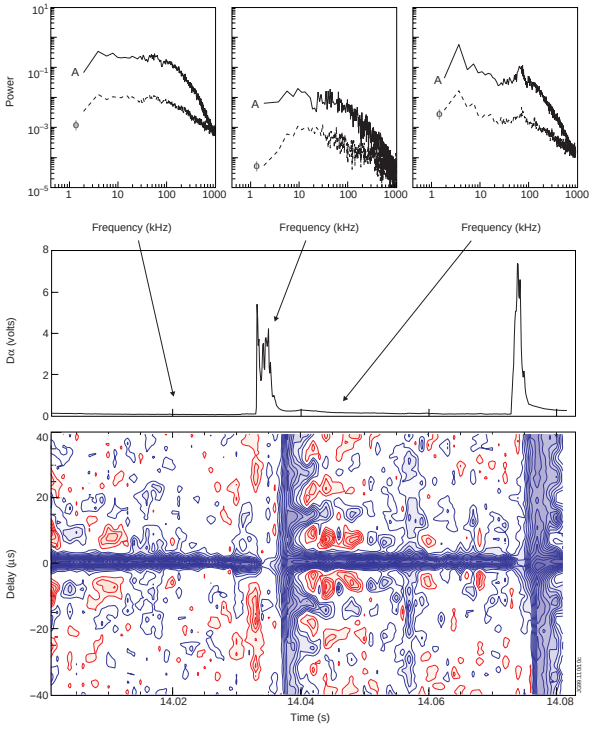

Fig.12: Contour plot of time-delayed correlation coefficient between amplitude fluctuations from two toroidally separated channels of an ELMy H-mode (shot #38102). The Dα trace shows two type-I ELMs and the three Fourier spectra show turbulence levels before, during and after the first ELM.

After each ELM the turbulence re-establishes on a time-scale of 3 - 4ms, with the lower frequencies recovering first. This is suggestive of energy cascading from longer to shorter wavelengths, although of course the plasma rotation velocity also receives a 'hicup' during the ELM which might account for some of the frequency shift. The wide `striation' in the correlation after the ELM corresponds to a 2kHz oscillation, which is also seen on the SXR cameras, followed by a strong coherent post-cursor, or ringing mode at 75kHz lasting some 12ms or more. Post-cursor modes are very often observed, but pre-cursor MHD modes are hardly ever seen, in either the magnetic or the reflectometer signals. The radial correlation also shows the same turbulence collapse, recovery, striation and post-cursor mode.

8. DISCUSSION

The correlation reflectometer system described in this paper has many features which make it a versatile tool for the collection of density fluctuation data in a difficult experimental environment with only modest access. The principal features are:

1. the ability to select between poloidal or toroidal correlation measurements using the same microwave circuitry without intervention in the machine hall,
2. the ability to combine these measurements with simultaneous radial measurements using the same antennae, and
3. the ability to separate amplitude and phase fluctuations on all channels.

In addition, the ability to sample on three time-scales ranging from one fast enough to observe the time evolution of microturbulence induced fields, to one slow enough to provide an overview of the long JET pulses, allows a guided and efficient exploration of the plasma fluctuation phenomena.

A small selection of results were presented to illustrate the capabilities (and limitations) of the diagnostic. Although some care is required in the interpretation of two-point correlation measurements due to the multiplicity of toroidal and radial effects that can occur [11], the results show that two point measurements are more than capable of providing practical estimates of

correlation and propagation properties in most circumstances. While some form of 'imaging' reflectometer might avoid some of the limitations of two-point measurements for long wavelength turbulence, it is questionable whether such a diagnostic would be practical (financially and technically) for a large fusion device.

An important result obtained from this diagnostic is that the phase and amplitude fluctuations do not always display the same phenomena. Temporal variations in the correlation between the phase fluctuations are often out of synchronization with the correlation between power fluctuations, i.e. when the phase correlation is high the amplitude correlation is low, and visa versa. Simulation studies [24] suggest that this may in fact be an inherent characteristic of the reflectometer diagnostic.

ACKNOWLEDGMENTS

Special acknowledgements to Gennadiy Ermak (IRE) and Daniel Korneev (ELVA-1 Ltd.) for detailed design and construction of the microwave electronics and hardware for two of the subsystems. Thanks also to members of the JET Team during the 1995 to 1997 experimental campaigns, and to N.Deliyanakis for assistance.

REFERENCES

[1] A.E.Costley and P.Cripwell, Proc. Wksp. on Electrostatic Turbulence, Cadarache, France, Report EUR-CEA-FC-1381 (1989). Also released as report JET-P(89)92 (1989)

[2] P.Cripwell, A.E.Costley, and A.E.Hubbard, Proc. 16th EPS Eur. Conf. on Contl. Fusion and Plasma Phys., Venice, ECA Vol.13B, Pt.I, 75 (1989)

[3] G.R.Hanson, J.B.Wilgen, E.Anabitarte *et al*., Rev. Sci. Instrum. **61**, 3049 (1990)

[4] P.Cripwell and A.E.Costley, Proc. 18th EPS Eur. Conf. on Contl. Fusion and Plasma Phys., Berlin, ECA Vol.15C, Pt.I, 17 (1991)

[5] T.L.Rhodes, W.A.Peebles, and E.J.Doyle, Rev. Sci. Instrum. **63**, 4661 (1992)

[6] P.Cripwell, A.E.Costley and T.Fukuda, Proc. IAEA Tech. Comm. Meeting on Microwave Reflectometry (JET), Vienna, p168 (1992). A.E.Costley, P.Cripwell and T.Fukuda, Proc. 19th Eur. Conf. on Contl. Fusion and Plasma Phys., Innsbruck, ECA Vol.16C, Pt.I, 199 (1992)

[7] G.R.Hanson, J.H.Harris, J.B.Wilgen *et al*., Nucl. Fusion **32**, 1593 (1992)

[8] J.Sanchez, B.Brana, E.de la Luna, and T.Estrada, Rev. Sci. Instrum. **64**, 487 (1993)

[9] V.A.Vershkov, V.V.Dreval and S.V.Soldatov, Proc. of 21st EPS Eur. Conf. on Cont. Fusion and Plasma Phys., Montpellier, ECA Vol.18B, Pt.III, 1192 (1994)

[10] T.L.Rhodes, R.J.Taylor, and W.A.Peebles, Rev. Sci. Instrum. **66**, 824 (1995)

[11] A.E.Costley, P.Cripwell, and G.Vayakis, Proc. 1993 Wksp. on Local Transport Studies in Fusion Plasmas, Varenna (1993) also JET Report JET-P(93)102 (1993)

[12] V.A.Vershkov, A.A.Bagdasorov, N.L.Vasin *et al*. Proc. 20th EPS Eur. Conf. on Cont. Fusion and Plasma Phys., Lisoba, ECA Vol. 17C, Pt. I, 20 (1993)

[13] M.Frances, T.Estrada, J.Sanchez, V.Zhuravlev, E.de la Luna, and B.Branas, Proc. 22nd EPS Eur. Conf. on Cont. Fusion and Plasma Phys., Bournemouth, ECA Vol.19C, Pt.IV, 429 (1995)

[14] A.Yu.Stepanov, V.N.Budnikov, E.Z.Gusakov, L.A.Esipov, E.R.Its and V.Yu. Shorikov, Proc. 23rd EPS Eur. Conf. on Cont. Fusion and Plasma Phys., Kiev, ECA Vol.20C, Pt.III, 1068 (1996)

[15] G.Vayakis, Proc. 2nd IAEA Tech. Meeting on Microwave Reflectometry, Princeton, USA (1994)

[16] Supplied by Institute of Radiophysics and Electronics NAS (IRE), 12 Ak. Proskura Str., 310085 Kharkov, Ukraine. email: ermak@ire.kharkov.ua

[17] Supplied by Millimetre Wave division, ELVA-1 Ltd., (DOK Ltd.) Nevsky 74, 23N St. Petersburg, Russia. http://www.nienschanz.ru/elva-1

[18] G.D.Conway, Plasma Phys. Contrl. Fusion **39**, 1261 (1997)

[19] K.Blackler and A.W.Edwards, IEEE Trans. Nucl. Sci. **41**, 111 (1994)

[20] G.D.Conway, '2D physical optics simulation of fluctuation reflectometry', III Wksp. on Microwave Reflectometry for Fusion Plasma Diagnostics, Madrid, Report Informes Tecnicos Ciemat **838**, p39 (1997). Also JET report JET-P(97)14.

[21] G.D.Conway, G.Vayakis and D.V.Bartlett, 'Reflectometer fluctuation and correlation studies on JET', III Wksp. on Microwave Reflectometry for Fusion Plasma Diagnostics, Madrid, Report Informes Tecnicos Ciemat **838**, p1 (1997). Also JET report JET-P(97)13.

[22] N.Iwama, Y.Ohba and T.Tsukishima, J. Appl. Phys. **50**, 3197 (1979)

[23] G.D.Conway and J.A.Elliott, J. Phys. E: Sci. Instrum. **20**, 1341 (1987)

[24] G.D.Conway, Plasma Phys. Contrl. Fusion **39**, 407 (1997)